Action-Conditioned 3D Human Motion Synthesis with Transformer VAE

Mathis Petrovich[1] Michael J. Black[2] Gül Varol[1]
[1] LIGM, École des Ponts, Univ Gustave Eiffel, CNRS, France
[2] Max Planck Institute for Intelligent Systems, Tübingen, Germany
{mathis.petrovich,gul.varol}@enpc.fr, black@tue.mpg.de
https://imagine.enpc.fr/~petrovim/actor

Abstract

We tackle the problem of action-conditioned generation of realistic and diverse human motion sequences. In contrast to methods that complete, or extend, motion sequences, this task does not require an initial pose or sequence. Here we learn an action-aware latent representation for human motions by training a generative variational autoencoder (VAE). By sampling from this latent space and querying a certain duration through a series of positional encodings, we synthesize variable-length motion sequences conditioned on a categorical action. Specifically, we design a Transformer-based architecture, ACTOR, for encoding and decoding a sequence of parametric SMPL human body models estimated from action recognition datasets. We evaluate our approach on the NTU RGB+D, HumanAct12 and UESTC datasets and show improvements over the state of the art. Furthermore, we present two use cases: improving action recognition through adding our synthesized data to training, and motion denoising. Our code and models will be made available.

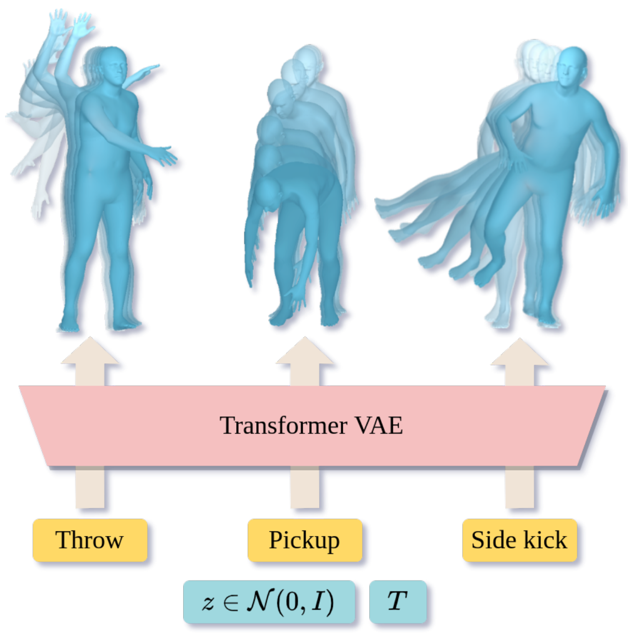

Figure 1: **Goal:** We learn an Action-Conditioned TransfORmer VAE (ACTOR) to synthesize human motion sequences conditioned on a categorical action and a duration, T. Sequences are generated by sampling from a single motion representation latent vector, z, as opposed to the frame-level embedding space in prior work.

1. Introduction

Despite decades of research on modeling human motions [6, 7], synthesizing realistic and controllable sequences remains extremely challenging. In this work, our goal is to take a semantic action label like "Throw" and generate an infinite number of realistic 3D human motion sequences, of varying length, that look like realistic throwing (Figure 1). A significant amount of prior work has focused on taking one pose, or a sequence of poses, and then predicting future motions [5, 8, 25, 61, 63]. This is an overly constrained scenario because it assumes that one already has a motion sequence and just needs more of it. On the other hand, many applications such as virtual reality and character control [29, 55] require generating motions of a given type (semantic action label) with a specified duration.

We address this problem by training an action-conditioned generative model with 3D human motion data that has corresponding action labels. In particular, we construct a Transformer-based encoder-decoder architecture and train it with the VAE objective. We show the importance of several reconstruction loss terms that impose constraints on the parametric representation of 3D motions, using the SMPL body model [42]. Our results suggest that the loss on joint coordinates alone, or rotations in the kinematic tree, are not sufficient for a realistic generation, but that their combination proves effective.

The key challenge of motion synthesis is to generate sequences that are perceptually realistic while being diverse. Many approaches for motion generation have taken an autoregressive approach such as LSTMs [19] and GRUs [45]. However, these methods typically regress to the mean pose after some time [45] and are subject to drift. The key novelty in our Transformer model is to provide positional encodings to the decoder and to output the full sequence at once. Positional encoding has been popularized by recent work on neural radiance fields [46]; we have not seen it used for motion generation as we do. This allows the generation of variable length sequences without the problem of the motions regressing to the mean pose. Moreover, our approach is to our knowledge the first to create an action-conditioned *sequence*-level embedding. The closest work is Action2Motion [24], which, in contrast, presents an autoregressive approach where the latent representation is at the *frame*-level.

A challenge specific to our action-condition generation problem is that there exists limited motion capture (MoCap) data paired with distinct action labels, typically on the order of 10 categories [2, 30]. We instead rely on monocular motion estimation methods [35] to obtain 3D sequences for actions and present promising results on 40 fine-grained categories of the UESTC action recognition dataset [31]. In contrast to [24], we do not require multi-view cameras to process monocular trajectory estimates, which makes our model potentially applicable to larger scales. Despite being noisy, monocular estimates prove sufficient for training and, as a side benefit of our model, we are able to denoise the estimated sequences by encoding-decoding through our learned motion representation.

An action-conditioned generative model can augment existing MoCap datasets, which are expensive and limited in size [2, 44]. Recent work, which renders synthetic human action videos for training action recognition models [58], shows the importance of motion diversity and large amounts of data per action. Such approaches can benefit from an infinite source of action-conditioned motion synthesis. We explore this through our experiments on action recognition. We observe that while having a domain gap, the generated motions can serve as additional training data, particularly in low-data regimes. Finally, a compact action-aware representation space for human motions can be used as a prior in other applications such as human motion estimation from videos.

Our contributions are fivefold: (i) We introduce ACTOR, a novel Transformer-based conditional VAE, and train it to generate action-conditioned human motions by sampling from a sequence-level latent vector. (ii) We show improved accuracy by using both the joint locations and rotations of a parametric body motion representation; (iii) We demonstrate that it is possible to learn to generate realistic 3D human motions using noisy 3D body poses estimated from monocular video; (iv) We present a comprehensive ablation study of the architecture and loss components, obtaining state-of-the-art performance on multiple datasets; (v) We illustrate two use cases for our model on action recognition and MoCap denoising. Code will be available for research purposes.

2. Related Work

We briefly review relevant literature on future motion prediction, motion synthesis, monocular motion estimation, as well as Transformers in the context of VAEs.

Future human motion prediction. Research on human motion analysis has a long history dating back to 1980s [7, 20, 22, 48]. Given past motion or initial pose, predicting the future frames has been referred as motion prediction. Statistical models have been employed in earlier studies [9, 21]. Recently, several works show promising results following progress in generative models with neural networks, such as GANs [23] or VAEs [34]. Examples include HP-GAN [8] and recurrent VAE [25] for future motion prediction. Most work treats the body as a skeleton, though recent work exploits full 3D body shape models [5, 63]. Similar to [63], we also go beyond sparse joints and incorporate vertices on the body surface. DLow [61] focuses on diversifying the sampling of future motions from a pretrained model. [14] performs conditional future prediction using contextual cues about the object interaction. Very recently, [38] presents a Transformer-based method for dance generation conditioned on music and past motion. Duan et al. [17] use Transformers for motion completion. There is a related line of work on motion "in-betweening" that takes both past and future poses and "inpaints" plausible motions between them; see [26] for more. In contrast to this prior work, our goal is to synthesize motions without any past observations.

Human motion synthesis. While there is a vast literature on future prediction, synthesis from scratch has received relatively less attention. Very early work used PCA [47] and GPLVMs [57] to learn statistical models of cyclic motions like walking and running. Conditioning synthesis on multiple, varied, actions is much harder. DVGANs [39] train a generative model conditioned on a short text representing actions in MoCap datasets such as Human3.6M [12, 30] and CMU [2]. Text2Action [3] and Language2Pose [4] similarly explore conditioning the motion generation on textual descriptions. Music-to-Dance [36] and [37] study music-conditioned generation. QuaterNet [51] focuses on generating locomotion actions such as walking, running given a ground trajectory and average speed. [59] presents a convolution-based generative model for realistic, but unconstrained motions without specifying an action. Similarly, [62] synthesizes arbitrary sequences, focusing on unbounded motions in time.

Many methods for unconstrained motion synthesis are often dominated by actions such as walking and running. In contrast, our model is able to sample from more general, acyclic, pre-defined action categories, compatible with ac-

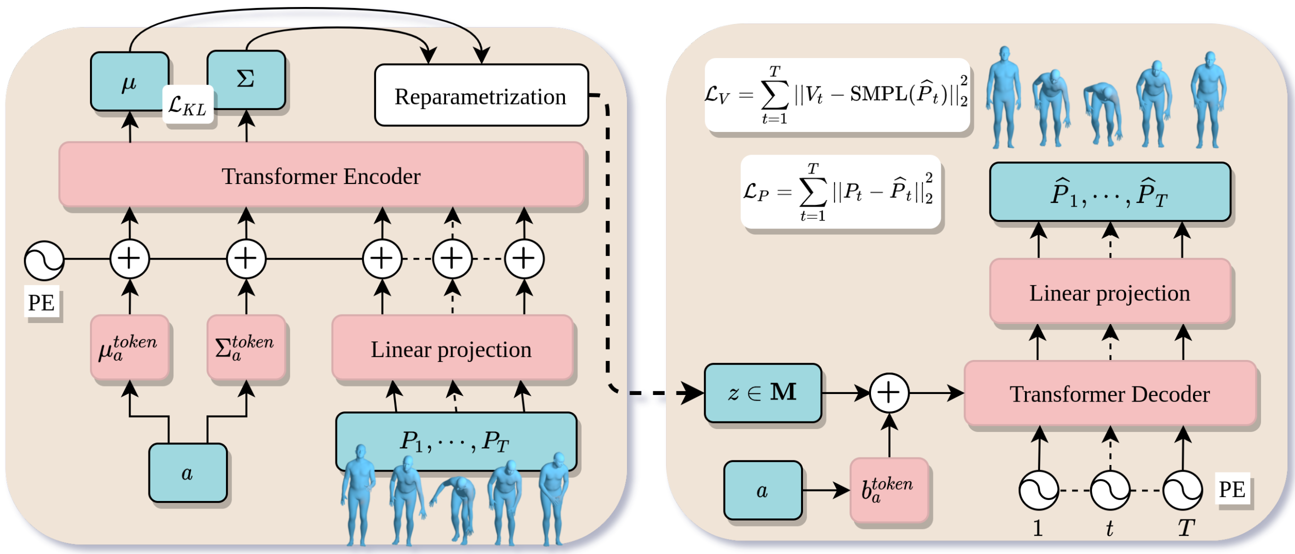

Figure 2: **Method overview:** We illustrate the encoder (left) and the decoder (right) of our Transformer-based VAE model to generate action-conditioned motions. Given a sequence of body poses $P_1, \ldots, P_T$ and an action label a, the encoder outputs distribution parameters on which we define a KL loss ($\mathcal{L}_{KL}$). We use extra learnable tokens per action (μ_a^{token} and Σ_a^{token}) as a way to obtain μ and Σ from the Transformer encoder. We sample from μ and Σ the motion latent representation $z \in \mathbf{M}$. The decoder takes the latent vector z, an action label a, and a duration T as input. The action determines the learnable b_a^{token} additive token, and the duration determines the number of positional encodings (PE) to input to the decoder. The decoder outputs the whole sequence $\widehat{P}_1, \ldots, \widehat{P}_T$ against which the reconstruction loss $\mathcal{L}_P$ is computed. In addition, we compute vertices with a differentiable SMPL layer to define a vertex loss ($\mathcal{L}_V$). For training z is obtained as the output of the encoder; for generation it is randomly sampled from a Gaussian distribution.

tion recognition datasets. In this direction, [64] introduces a Bayesian approach, where Hidden semi-Markov Models are used for jointly training generative and discriminative models. Similar to us, [64] shows that their generated motions can serve as additional training data for action recognition. However, their generated sequences are pseudo-labelled with actions according to the discriminator classification results. On the other hand, our conditional model can synthesize motions in a controlled way, e.g. balanced training set. Most similar to our work is Action2Motion [24], a *per-frame* variational autoencoder conditioned on actions, using a GRU-based architecture. Our sequence-level latent space, in conjunction with the Transformer-based design provides significant advantages, as shown in our experiments.

There is also a significant graphics literature on the topic, which tends to focus on animator control. See, for example, recent work on learning motion matching [28]. Most relevant here are the phase-functioned neural networks [29] and neural state machines [55]. Both exploit notion of actions being driven by the phase of a sinusoidal function. This is related to the idea of positional encoding, but unlike our approach, their methods require manual labor to segment actions and build these phase functions.

Monocular human motion estimation. Motion estimation from videos [33, 35, 43] has recently made significant progress but is beyond our scope. In this work, we adopt VIBE [35] to obtain training motion sequences from action-labelled video datasets.

Transformer VAEs. Recent success of Transformers in language tasks has increased interest in attention-based neural network models. Several works use Transformers in conjunction with generative VAE training. Particular examples include story generation [18], sentiment analysis [13], response generation [40], and music generation [32]. The work of [32] learns latent embeddings per timeframe, while [13] averages the hidden states to obtain a single latent code. On the other hand, [18] performs attention averaging to pool over time. In contrast to these works, we adopt learnable tokens as in [15, 16] to summarize the input into a sequence-level embedding.

3. Action-Conditioned Motion Generation

Problem definition. Actions defined by body-motions can be characterized by the rotations of body parts, independent of identity-specific body shape. To be able to generate motions with actors of different morphology, it is desirable to disentangle the pose and the shape. Consequently, we employ the SMPL body model [42], which is a disentangled body representation. Ignoring shape, our goal, is then to generate a sequence of *pose* parameters. More formally, given an action label a (from a set of predefined action categories $a \in A$) and a duration T, we generate a sequence of body poses $R_1, \ldots, R_T$ and a sequence of translations of the root joint represented as displacements, $D_1, \ldots, D_T$ (with $D_t \in \mathbb{R}^3, \forall t \in \{1, \ldots, T\}$).

Motion representation. SMPL pose parameters per-frame represent 23 joint rotations in the kinematic tree and one global rotation. We adopt the continuous 6D rotation representation for training [65], making $R_t \in \mathbb{R}^{24\times 6}$. Let P_t be the combination of R_t and D_t, representing the pose and location of the body in a single frame, t. The full motion is the sequence $P_1, \ldots, P_T$. Given a generator output pose P_t and any shape parameter, we can obtain body mesh vertices (V_t) and body joint coordinates (J_t) differentiably using [42].

3.1. Conditional Transformer VAE for Motions

We employ a conditional variational autoencoder (CVAE) model [54] and input the action category information to both the encoder and the decoder. More specifically, our model is an action-conditioned Transformer VAE (ACTOR), whose encoder and decoder consist of Transformer layers (see Figure 2 for an overview).

Encoder. The encoder takes an arbitrary-length sequence of poses, and an action label a as input, and outputs distribution parameters μ and Σ of the motion latent space. Using the reparameterization trick [34], we sample from this distribution a latent vector $z \in \mathbf{M}$ with $\mathbf{M} \subset \mathbb{R}^d$. All the input pose parameters (R) and translations (D) are first linearly embedded into a $\mathbb{R}^d$ space. As we embed arbitrary-length sequences into one latent space (sequence-level embedding), we need to pool the temporal dimension. In other domains, a `[class]` token has been introduced for pooling purposes, e.g., in NLP with BERT [15] and more recently in computer vision with ViT [16]. Inspired by this approach, we include two extra learnable parameters per action, μ_a^{token} and Σ_a^{token}, which are distribution parameter tokens. We append the embedded pose sequences to these tokens. The resulting Transformer encoder input is the summation with the positional encodings in the form of sinusoidal functions. We obtain the distribution parameters μ and Σ by taking the first two outputs of the encoder corresponding to the distribution parameter tokens (i.e., discarding the rest).

Decoder. Given a single latent vector z and an action label a, the decoder generates a realistic human motion for a given duration. Note that we do not use an autoregressive decoder as we found this type of model difficult to train, mainly due to teacher forcing resulting in a mismatch between training and testing. We use a Transformer decoder model where we feed time information as a query (in the form of T sinusoidal positional encoding), and the latent vector combined with action information, as key and value. To incorporate the action information, we simply add a learnable bias b_a^{token} to shift the latent representation to an action-dependent space. The Transformer decoder outputs a sequence of T vectors in $\mathbb{R}^d$ from which we obtain the final poses $\widehat{P}_1, \ldots, \widehat{P}_T$ following a linear projection. A differentiable SMPL layer is used to obtain vertices and joints given the pose parameters as output by the decoder.

3.2. Training

We define several loss terms to train our model and present an ablation study in Section 4.2.

Reconstruction loss on pose parameters ($\mathcal{L}_P$). We use an L2 loss between the ground-truth poses $P_1, \ldots, P_T$, and our predictions $\widehat{P}_1, \ldots, \widehat{P}_T$ as $\mathcal{L}_P = \sum_{t=1}^{T} \|P_t - \widehat{P}_t\|_2^2$. Note that this loss contains both the SMPL rotations and the root translations. When we experiment by discarding the translations, we break this term into two: $\mathcal{L}_R$ and $\mathcal{L}_D$, for rotations and translations, respectively.

Reconstruction loss on vertex coordinates ($\mathcal{L}_V$). We feed the SMPL poses P_t and $\widehat{P}_t$ to a differentiable SMPL layer (without learnable parameters) with a mean shape (i.e., $\beta = \vec{0}$) to obtain the root-centered vertices of the mesh V_t and $\widehat{V}_t$. We define an L2 loss by comparing to the ground-truth vertices V_t as $\mathcal{L}_V = \sum_{t=1}^{T} \|V_t - \widehat{V}_t\|_2^2$. We further experiment with a loss $\mathcal{L}_J$ on a more sparse set of points such as joint locations $\widehat{J}_t$ obtained through the SMPL joint regressor. However, as will be shown in Section 4.2, we do not include this term in the final model.

KL loss ($\mathcal{L}_{KL}$). As in a standard VAE, we regularize the latent space by enforcing it to be similar to a Gaussian distribution. We minimize the Kullback–Leibler (KL) divergence between the encoder distribution and the normal distribution.

The resulting total loss is defined as the summation of different terms: $\mathcal{L} = \mathcal{L}_P + \mathcal{L}_V + \lambda_{KL}\mathcal{L}_{KL}$. We empirically show the importance of weighting with λ_{KL} in our experiments to obtain a good trade-off between diversity and realism (see Section A.1 of the appendix). The remaining loss terms are simply equally weighed, further improvements are potentially possible with tuning. We use the AdamW optimizer with a fixed learning rate of 0.0001. The minibatch size is set to 20 and we found that the performance is sensitive to this hyperparameter (see Section A.2 of the appendix). We train our model for 2000, 5000 and 1000 epochs on NTU-13, HumanAct12 and UESTC datasets, respectively. Overall, more epochs produce improved performance, but we stop training to retain a low computational cost. Note that to allow faster iterations, for ablations on loss and architecture, we train our models for 1000 epochs on NTU-13 and 500 epochs on UESTC. The remaining implementation details can be found in Section C of the appendix.

4. Experiments

We first introduce the datasets and performance measures used in our experiments (Section 4.1). Next, we present an ablation study (Section 4.2) and compare to previous work (Section 4.3). Then, we illustrate use cases in action recognition (Sections 4.4). Finally, we provide qualitative results and discuss limitations (Section 4.5).

	UESTC					NTU-13			
Loss	FID$_{tr}$↓	FID$_{test}$↓	Acc.↑	Div.→	Multimod.→	FID$_{tr}$↓	Acc.↑	Div.→	Multimod.→
Real	$2.93^{\pm 0.26}$	$2.79^{\pm 0.29}$	$98.8^{\pm 0.1}$	$33.34^{\pm 0.32}$	$14.16^{\pm 0.06}$	$0.02^{\pm 0.00}$	$99.8^{\pm 0.0}$	$7.07^{\pm 0.02}$	$2.27^{\pm 0.01}$
$\mathcal{L}_J$	3M	3M	$3.3^{\pm 0.2}$	$267.68^{\pm 346.06}$	$153.62^{\pm 50.62}$	$0.49^{\pm 0.00}$	$93.6^{\pm 0.2}$	$7.04^{\pm 0.04}$	$2.12^{\pm 0.01}$
$\mathcal{L}_R$	$292.54^{\pm 113.35}$	$316.29^{\pm 26.05}$	$42.4^{\pm 1.7}$	$23.16^{\pm 0.47}$	$14.37^{\pm 0.08}$	$0.23^{\pm 0.00}$	$95.4^{\pm 0.2}$	$7.08^{\pm 0\ .04}$	$2.18^{\pm 0.02}$
$\mathcal{L}_V$	4M	4M	$2.7^{\pm 0.2}$	$314.66^{\pm 476.18}$	$169.49^{\pm 27.90}$	$0.25^{\pm 0.00}$	$95.8\ ^{\pm 0.3}$	$7.08^{\pm 0.04}$	$2.07^{\pm 0.01}$
$\mathcal{L}_R$ + $\mathcal{L}_V$	$\mathbf{20.49}^{\pm 2.31}$	$\mathbf{23.43}^{\pm 2.20}$	$\mathbf{91.1}^{\pm 0.3}$	$31.96^{\pm 0.36}$	$14.66^{\pm 0.03}$	$\mathbf{0.19}^{\pm 0.00}$	$\mathbf{96.2}^{\pm 0.2}$	$7.09^{\pm 0.04}$	$2.08^{\pm 0.01}$

Table 1: **Reconstruction loss:** We define the loss on the SMPL pose parameters which represent the rotations in the kinematic tree ($\mathcal{L}_R$), their joint coordinates ($\mathcal{L}_J$), as well as vertex coordinates ($\mathcal{L}_V$). We show that constraining both rotations and vertex coordinates is critical to obtain smooth motions. In particular, coordinate-based losses alone do not converge to a meaningful solution on UESTC. → means motions are better when the metric is closer to real.

4.1. Datasets and evaluation metrics

We use three datasets originally proposed for action recognition, mainly for skeleton-based inputs. Each dataset is temporally trimmed around one action per sequence. Next, we briefly describe them.

NTU RGB+D dataset [41, 53]. To be able to compare to the work of [24], we use their subset of 13 action categories. [24] provides SMPL parameters obtained through VIBE estimations. Their 3D root translations obtained through multi-view constraints is however not publicly available, therefore we use their approximately origin-centered version. We refer to this data as NTU-13 and use it for training.

HumanAct12 dataset [24]. Similarly, we use this data for state-of-the-art comparison. HumanAct12 is adapted from the PHSPD dataset [66] that releases SMPL pose parameters and root translations in camera coordinates for 1191 videos. HumanAct12 temporally trims the videos, annotates them into 12 action categories, and only provides their joint coordinates in a canonical frame. We also process the SMPL poses to align them to the frontal view.

UESTC dataset [31]. This recent dataset consists of 25K sequences across 40 action categories (mostly exercises, and some represent circular movements). To obtain SMPL sequences, we apply VIBE on each video and select the person track that corresponds best to the Kinect skeleton provided in case there are multiple people. We use all 8 static viewpoints from 24K (we discard the rotating camera) and canonicalize all bodies to the frontal view. We use the official cross-subject protocol to separate train and test splits, instead of the cross-view protocols since generating different viewpoints is trivial for our model. This results in 10650 training sequences that we use for learning the generative model, as well as the recognition model. The remaining 13350 sequences are used for testing. Since the protocols on NTU-13 and HumanAct12 do not provide test splits, we rely on the UESTC dataset for recognition experiments.

Evaluation metrics. We follow the performance measures employed in [24] for quantitative evaluations. We measure FID, action recognition accuracy, overall diversity, and per-action diversity (referred to as multimodality in [24]). For all these metrics, a pretrained action recognition model is used, either for extracting motion features to compute FID, diversity, and multimodality; or directly the accuracy of recognition. For experiments on NTU-13 and HumanAct12, we directly use the provided recognition models of [24] that operate on joint coordinates. For UESTC, we train our own recognition model based on pose parameters expressed as 6D rotations (we observed that the joint-based models of [24] are sensitive to global viewpoint changes). We generate sets of sequences 20 times with different random seeds and report the average together with the confidence interval at 95%. We refer to [24] for further details. One difference in our evaluation is the use of average shape parameter ($\beta = \vec{0}$) when obtaining joint coordinates from the mesh for both real and generated sequences. Note also that [24] only reports FID score comparing to the training split (FID$_{tr}$), since NTU-13 and HumanAct12 datasets do not provide test splits. On UESTC, we additionally provide an FID score on the test split as FID$_{test}$, which we rely most on to make conclusions.

4.2. Ablation study

We first ablate several components of our approach in a controlled setup, studying the loss and the architecture.

Loss study. Here, we investigate the influence of the reconstruction loss formulation when using the parametric SMPL body model in our VAE. We first experiment with using (i) only the rotation parameters $\mathcal{L}_R$, (ii) only the joint coordinates $\mathcal{L}_J$, (iii) only the vertex coordinates $\mathcal{L}_V$, and (iv) the combination $\mathcal{L}_R + \mathcal{L}_V$. Here, we initially discard the root translation to only assess the pose representation. Note that for representing the rotation parameters, we use the 6D representation from [65] and further loss study on different rotation representations can be found in Section A.4 of the appendix. In Table 1, we observe that a single loss is not sufficient to constrain the problem, especially losses on the coordinates do not converge to a meaningful solution on UESTC. On NTU-13, qualitatively, we also observe that a single loss term produces motions with significant jitter while they are not reflected in the metrics. We provide examples in our qualitative analysis. We conclude that using a

Architecture	UESTC FID$_{tr}$↓	UESTC FID$_{test}$↓	UESTC Acc.↑	UESTC Div.→	UESTC Multimod.→	NTU-13 FID$_{tr}$↓	NTU-13 Acc.↑	NTU-13 Div.→	NTU-13 Multimod.→
Real	$2.93^{\pm0.26}$	$2.79^{\pm0.29}$	$98.8^{\pm0.1}$	$33.34^{\pm0.32}$	$14.16^{\pm0.06}$	$0.02^{\pm0.00}$	$99.8^{\pm0.0}$	$7.07^{\pm0.02}$	$2.27^{\pm0.01}$
Fully connected	$562.09^{\pm48.12}$	$548.13^{\pm38.34}$	$10.5^{\pm0.5}$	$12.96^{\pm0.11}$	$10.87^{\pm0.05}$	$0.47^{\pm0.00}$	$88.7^{\pm0.6}$	$6.93^{\pm0.03}$	$3.05^{\pm0.01}$
GRU	$25.96^{\pm3.02}$	$27.08^{\pm2.98}$	$87.3^{\pm0.4}$	$30.66^{\pm0.33}$	$15.24^{\pm0.08}$	$0.28^{\pm0.00}$	$94.8^{\pm0.2}$	$7.08^{\pm0.04}$	$2.20^{\pm0.01}$
Transformer	$\mathbf{20.49}^{\pm2.31}$	$\mathbf{23.43}^{\pm2.20}$	$\mathbf{91.1}^{\pm0.3}$	$31.96^{\pm0.36}$	$14.66^{\pm0.03}$	$0.19^{\pm0.00}$	$\mathbf{96.2}^{\pm0.2}$	$7.09^{\pm0.04}$	$2.08^{\pm0.01}$
w/out $\mu_a^{token}, \Sigma_a^{token}$	$27.46^{\pm3.43}$	$31.37^{\pm3.04}$	$86.2^{\pm0.4}$	$31.82^{\pm0.38}$	$15.71^{\pm0.12}$	$0.26^{\pm0.00}$	$94.7^{\pm0.2}$	$7.09^{\pm0.03}$	$2.15^{\pm0.01}$
w/out b_a^{token}	$24.38^{\pm2.37}$	$28.52^{\pm2.55}$	$89.4^{\pm0.7}$	$32.11^{\pm0.33}$	$14.52^{\pm0.09}$	$\mathbf{0.16}^{\pm0.00}$	$\underline{96.2}^{\pm0.2}$	$7.08^{\pm0.04}$	$2.19^{\pm0.02}$

Table 2: **Architecture:** We compare various architectural designs, such as the encoder and the decoder of the VAE, and different components of the Transformer model, on both NTU-13 and UESTC datasets.

combined loss significantly improves the results, constraining the pose space more effectively. We further provide an experiment on the influence of the weight parameter λ_{KL} controlling the KL divergence loss term $\mathcal{L}_{KL}$ in Section A.1 of the appendix and note its importance to obtain high diversity performance.

Root translation. Since we estimate the 3D human body motion from a monocular camera, obtaining the 3D trajectory of the root joint is not trivial for real training sequences, and is subject to depth ambiguity. We assume a fixed focal length and approximate the distance from the camera based on the ratio between the 3D body height and the 2D projected height. Similar to [58], we observe reliable translation in xy image plane, but considerable noise in z depth. Nevertheless, we still train with this type of data and visualize generated examples in Figure 3 with and without the loss on translation $\mathcal{L}_D$. Certain actions are defined by their trajectory (e.g., 'Left Stretching') and we are able to generate the semantically relevant translations despite noisy data. Compared to the real sequences, we observe much less noise in our generated sequences (see the supplemental video at [1]).

Architecture design. Next, we ablate several architectural choices. The first question is whether an attention-based design (i.e., Transformer) has advantages over the more widely used alternatives such as a simple fully-connected autoencoder or a GRU-based recurrent neural network. In Table 2, we see that our Transformer model outperforms both fully-connected and GRU encoder-decoder architecture on two datasets by a large margin.

We also provide a controlled experiment by changing certain blocks of our Transformer VAE. Specifically, we remove the μ_a^{token} and Σ_a^{token} distribution parameter tokens and instead obtain μ and Σ by averaging the outputs of the encoder, followed by two linear layers. This results in considerable drop in performance. Moreover, we investigate the additive b_a^{token} token and replace it with a one-hot encoding of the action label concatenated to the latent vector, followed by a linear projection. While this does not influence the results on the NTU-13 dataset, we observe an improvement in the UESTC dataset that has a larger number of action categories.

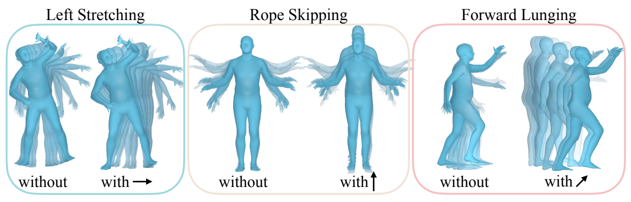

Figure 3: **Generating the 3D root translation:** Despite our model learning from noisy 3D trajectories, we show that our generations are smooth and they capture the semantics of the action. Examples are provided from the UESTC dataset for translations in x ('Left Stretching'), y (Rope Skipping), and z ('Forward Lugging') with and without the loss on the root displacement $\mathcal{L}_D$.

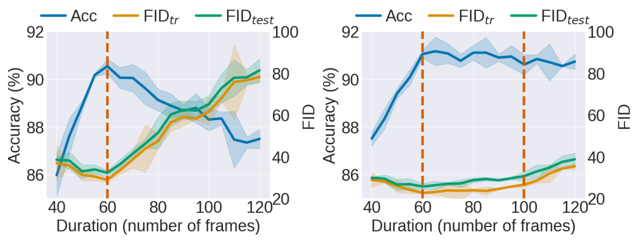

Figure 4: **Generating variable-length sequences:** We evaluate the capability of the models trained on UESTC with **(left)** fixed-size 60 frames and **(right)** variable-size between [60, 100] frames on generating various durations. We report accuracy and FID metrics. For the fixed model, we observe that the best performance is when tested at the seen duration of 60, but over 85% accuracy is retained even at ranges between [40, 120] frames. The performance is overall improved when the model has previously seen duration variations in training, with still a drop in performance beyond the seen range (denoted with dashed lines).

An architectural ablation about the number of Transformer layers is provided in Section A.3 of the appendix, where we set this parameter to 8.

Training with sequences of variable durations. A key advantage of sequence-modeling with architectures such as Transformers is to be able to handle variable-length motions. At generation time, we control how long the model should synthesize, by specifying a sequence of positional encodings to the decoder. We can trivially generate more

Method	NTU-13 FID$_{tr}$↓	NTU-13 Acc.↑	NTU-13 Div.→	NTU-13 Multimod.→	HumanAct12 FID$_{tr}$↓	HumanAct12 Acc.↑	HumanAct12 Div.→	HumanAct12 Multimod.→
Real [24]	$0.03^{\pm0.00}$	$99.9^{\pm0.1}$	$7.11^{\pm0.05}$	$2.19^{\pm0.03}$	$0.09^{\pm0.01}$	$99.7^{\pm0.1}$	$6.85^{\pm0.05}$	$2.45^{\pm0.04}$
Real*	$0.02^{\pm0.00}$	$99.8^{\pm0.0}$	$7.07^{\pm0.02}$	$2.25^{\pm0.01}$	$0.02^{\pm0.00}$	$99.4^{\pm0.0}$	$6.86^{\pm0.03}$	$2.60^{\pm0.01}$
CondGRU ([24]†)	$28.31^{\pm0.14}$	$7.8^{\pm0.1}$	$3.66^{\pm0.02}$	$3.58^{\pm0.03}$	$40.61^{\pm0.14}$	$8.0^{\pm0.2}$	$2.38^{\pm0.02}$	$2.34^{\pm0.04}$
Two-stage GAN [11] ([24]†)	$13.86^{\pm0.09}$	$20.2^{\pm0.3}$	$5.33^{\pm0.04}$	$3.49^{\pm0.03}$	$10.48^{\pm0.09}$	$42.1^{\pm0.6}$	$5.96^{\pm0.05}$	$2.81^{\pm0.04}$
Act-MoCoGAN [56] ([24]†)	$2.72^{\pm0.02}$	$\mathbf{99.7}^{\pm0.1}$	$6.92^{\pm0.06}$	$0.91^{\pm0.01}$	$5.61^{\pm0.11}$	$79.3^{\pm0.4}$	$6.75^{\pm0.07}$	$1.06^{\pm0.02}$
Action2Motion [24]	$0.33^{\pm0.01}$	$94.9^{\pm0.1}$	$7.07^{\pm0.04}$	$2.05^{\pm0.03}$	$2.46^{\pm0.08}$	$92.3^{\pm0.2}$	$7.03^{\pm0.04}$	$2.87^{\pm0.04}$
ACTOR (ours)	$\mathbf{0.11}^{\pm0.00}$	$97.1^{\pm0.2}$	$7.08^{\pm0.04}$	$2.08^{\pm0.01}$	$\mathbf{0.12}^{\pm0.00}$	$\mathbf{95.5}^{\pm0.8}$	$6.84^{\pm0.03}$	$2.53^{\pm0.02}$

Table 3: **State-of-the-art comparison:** We compare to the recent work of [24] on the NTU-13 and HumanAct12 datasets. Note that due to differences in implementation (e.g., random sampling, using zero shape parameter), our metrics for the ground truth real data (Real*) are slightly different than the ones reported in their paper. The performance improvement with our Transformer-based model shows a clear gap from Action2Motion. † Baselines implemented by [24].

diversity by synthesizing sequences of different durations. However, so far we have trained our models with a fixed-size inputs, i.e., 60 frames. Here, we first analyze whether a fixed-size trained model can directly generate variable sizes. This is presented in Figure 4 (left). We plot the performance over several sets of generations of different lengths between 40 and 120 frames (with a step size of 5). Since our recognition model used for evaluation metrics is trained on fixed-size 60-frame inputs, we naturally observe performance decrease outside of this length. However, the accuracy still remains high which indicates that our model is already capable of generating diverse durations.

Next, we *train* our generative model with variable-length inputs by randomly sampling a sequence between 60 and 100 frames. However, simply training this way from random weight initialization converges to a poor solution, leading to all generated motions to be frozen in time. We address this by pretraining at 60-frame fixed size and finetuning at variable sizes. We see in Figure 4 (right) that the performance is greatly improved with this model.

Furthermore, we investigate how the generations longer or shorter than their average durations behave. We observe qualitatively that shorter generations produce incomplete actions, e.g., picking up without reaching the floor, and longer generations slow down somewhat non-uniformly in time. We refer to the supplemental video at [1] for qualitative results.

4.3. Comparison to the state of the art

Action2Motion [24] is the only prior work that generates action-conditioned motions. We compare to them in Table 3 on their NTU-13 and HumanAct12 datasets. On both datasets, we obtain significant improvements over this prior work that uses autoregressive GRU blocks, as well as other baselines implemented by [24] by adapting other works [11, 56]. The main advantage of ACTOR is to exploit multiple losses for reconstruction and not relying on an autoregressive design. Besides the quantitative performance improvement, measured with recognition models based on joint coordinates, our model directly outputs SMPL pose parameters, which can further be diversified with varying the shape parameters. [24] instead applies an optimization step to fit SMPL models on their generated joint coordinates, which is typically substantially slower than a neural network forward pass.

	Test accuracy (%) Real$_{orig}$	Test accuracy (%) Real$_{denoised}$
Real$_{orig}$	91.8	93.2
Real$_{denoised}$	83.8	97.0
Real$_{interpolated}$	77.6	93.9
Generated	80.7	97.0
Real$_{orig}$ + Generated	**91.9**	**98.3**

Table 4: **Action recognition:** We employ a standard architecture (ST-GCN [60]) and perform action recognition experiments using several sets of training data on the UESTC cross-subject protocol [31]. Training only with generated samples obtains 80% accuracy on the real test set which is another indication our action-conditioning performs well. Nevertheless, we observe a domain gap between generated and real samples, mainly due to the noise present in the real data. We show that simply by encoding-decoding the test sequences, we observe a denoising effect, which in turn shows better performance. However, one should note that the last-column experiments are not meant to improve performance in the benchmark since it uses the action label information.

4.4. Use cases in action recognition

In this section, we test the limits of our approach by illustrating the benefits of our generative model and our learned latent representation for the skeleton-based action recognition task. We adopt a standard architecture, ST-GCN [60], that employs spatio-temporal graph convolutions to classify actions. We show that we can use our latent encoding for denoising motion estimates and our generated sequences as

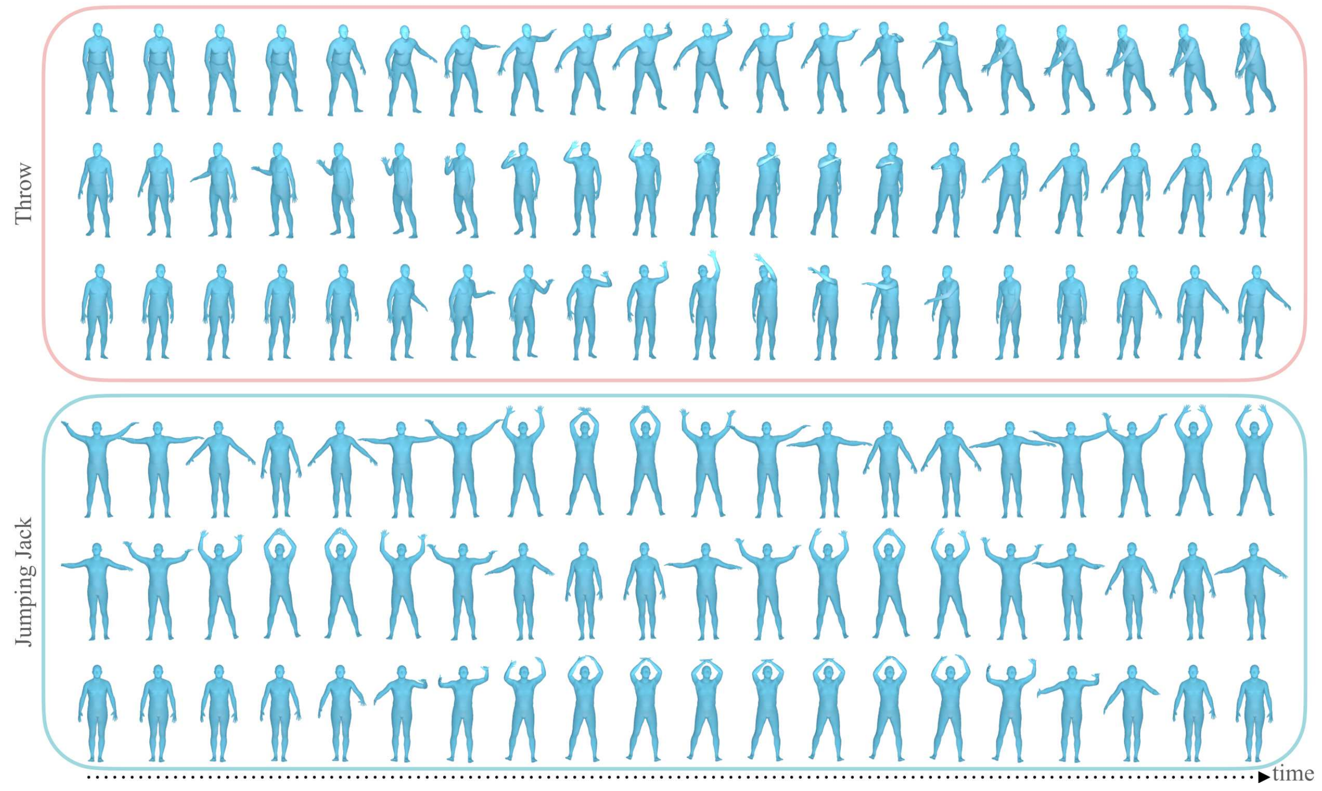

Figure 5: **Qualitative results:** We illustrate the diversity of our generations for two actions: 'Throw' action from NTU-13 (top) and 'Jumping Jack' action from UESTC (bottom). For each action, we show 3 generations. The horizontal axis represent the time axis and 20 equally spaced frames are visualized out of 60-frame generations. We demonstrate that our model is capable of generating different ways of performing a given action. More results can be found in Section B of the appendix and the supplemental video at [1].

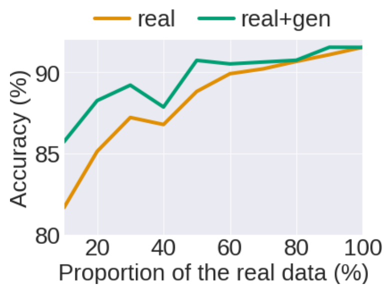

Figure 6: **Data augmentation:** We show the benefit of augmenting the real data with our generative model (real+gen), especially at low-data regime. We have limited gains when the real data is sufficiently large.

data augmentation to action recognition models.

Use case I: Human motion denoising. In the case when our motion data source relies on monocular motion estimation such as [35], the training motions remain noisy. We observe that by simply encoding-decoding the real motions through our learned embedding space, we obtain much cleaner motions. Since it is difficult to show motion quality results on static figures, we refer to our supplemental video at [1] to see this effect. We measure the denoising capability of our model through an action recognition experiment in Table 4. We change both the training and test set motions with the encoded-decoded versions. We show improved performance when trained and tested on Real$_{denoised}$ motions (97.0%) compared to Real$_{orig}$ (91.8). Note that this result on its own is not sufficient for this claim, but is only an indication since our decoder might produce less diversity than real motions. Moreover, the action label is given at denoising time. We believe that such denoising can be beneficial in certain scenarios where the action is known, e.g., occlusion or missing markers during MoCap collection.

Use case II: Augmentation for action recognition. Next, we augment the real training data (Real$_{orig}$), by adding generated motions to the training. We first measure the action recognition performance without using real sequences. We consider interpolating existing Real$_{orig}$ motions that fall within the same action category in our embedding space to create intra-class variations (Real$_{interpolated}$). We then synthesize motions by sampling noise vectors conditioned on each action category (Generated). Table 4 summarizes the results. Training only on synthetically generated data performs around 80% on the real test set, which is promising. However, there is a domain gap between the noisy real motions and our smooth generations. Consequently, adding generated motions to real training only marginally improves the performance.

In Figure 6, we investigate whether the augmented training helps for low-data regimes by training at several fractions of the data. In each minibatch we equally sample real and generated motions. However, in theory we have access to infinitely many generations. We see that the improvement is more visible at low-data regime.

4.5. Qualitative results

In Figure 5, we visualize several examples from our generations for two actions. We observe a great diversity in the way a given action is performed. For example, the 'Throw' action is performed with left or right hand. We also see different timings, e.g., different moments when the hands are raised in 'Jumping Jack' action. We refer to the supplemental video at [1] and Section B of the appendix for further qualitative analyses.

One limitation of our model is that the maximum duration it can generate depends on computational resources since we output all the sequence at once. Moreover, the actions are from a predefined set. Future work will explore open-vocabulary actions, which might become possible with further progress in 3D motion estimation from unconstrained videos.

5. Conclusions

We presented a new Transformer-based VAE model to synthesize action-conditioned human motions. We provided a detailed analysis to assess different components of our proposed approach. We obtained state-of-the-art performance on action-conditioned motion generation, significantly improving over prior work. Furthermore, we explored various use cases in motion denoising and action recognition. One especially attractive property of our method is that it operates on a sequence-level latent space. Future work can therefore exploit our model to impose priors on motion estimation or action recognition problems.

Acknowledgements. This work was granted access to the HPC resources of IDRIS under the allocation 2021-101535 made by GENCI. The authors would like to thank Mathieu Aubry and David Picard for helpful feedback, Chuan Guo and Shihao Zou for their help with Action2Motion details.
Disclosure: MJB has received research funds from Adobe, Intel, Nvidia, Facebook, and Amazon. While MJB is a part-time employee of Amazon, his research was performed solely at, and funded solely by, Max Planck. MJB has financial interests in Amazon, Datagen Technologies, and Meshcapade GmbH.

References

[1] ACTVAE project page: Action-conditioned 3D human motion synthesis with Transformer VAE. https://imagine.enpc.fr/~petrovim/actvae. 6, 7, 8, 9, 12

[2] Carnegie-Mellon Mocap Database. http://mocap.cs.cmu.edu/. 2

[3] Hyemin Ahn, Timothy Ha, Yunho Choi, Hwiyeon Yoo, and Songhwai Oh. Text2Action: Generative adversarial synthesis from language to action. In *ICRA*, 2018. 2

[4] Chaitanya Ahuja and Louis-Philippe Morency. Language2Pose: Natural language grounded pose forecasting. In *3DV*, 2019. 2

[5] Emre Aksan, Manuel Kaufmann, and Otmar Hilliges. Structured prediction helps 3D human motion modelling. In *ICCV*, 2019. 1, 2

[6] Norman Badler. *Temporal Scene Analysis: Conceptual Descriptions of Object Movements*. PhD thesis, University of Toronto, 1975. 1

[7] Norman I. Badler, Cary B. Phillips, and Bonnie Lynn Webber. *Simulating Humans: Computer Graphics Animation and Control*. Oxford University Press, Inc., New York, NY, USA, 1993. 1, 2

[8] Emad Barsoum, John Kender, and Zicheng Liu. HP-GAN: probabilistic 3D human motion prediction via GAN. In *CVPRW*, 2018. 1, 2

[9] R. Bowden. Learning statistical models of human motion. In *CVPRW*, 2000. 2

[10] Tom B. Brown, Benjamin Mann, Nick Ryder, Melanie Subbiah, Jared Kaplan, Prafulla Dhariwal, Arvind Neelakantan, Pranav Shyam, Girish Sastry, Amanda Askell, Sandhini Agarwal, Ariel Herbert-Voss, Gretchen Krueger, Tom Henighan, Rewon Child, Aditya Ramesh, Daniel M. Ziegler, Jeffrey Wu, Clemens Winter, Christopher Hesse, Mark Chen, Eric Sigler, Mateusz Litwin, Scott Gray, Benjamin Chess, Jack Clark, Christopher Berner, Sam McCandlish, Alec Radford, Ilya Sutskever, and Dario Amodei. Language models are few-shot learners. In *NeurIPS*, 2020. 12

[11] Haoye Cai, Chunyan Bai, Yu-Wing Tai, and Chi-Keung Tang. Deep video generation, prediction and completion of human action sequences. In *ECCV*, 2018. 7

[12] Cristian Sminchisescu Catalin Ionescu, Fuxin Li. Latent structured models for human pose estimation. In *ICCV*, 2011. 2

[13] Xingyi Cheng, Weidi Xu, Taifeng Wang, Wei Chu, Weipeng Huang, Kunlong Chen, and Junfeng Hu. Variational semi-supervised aspect-term sentiment analysis via transformer. In *Proceedings of the 23rd Conference on Computational Natural Language Learning (CoNLL)*, 2019. 3

[14] Enric Corona, Albert Pumarola, G. Alenyà, and F. Moreno-Noguer. Context-aware human motion prediction. In *CVPR*, 2020. 2

[15] J. Devlin, Ming-Wei Chang, Kenton Lee, and Kristina Toutanova. BERT: Pre-training of deep bidirectional transformers for language understanding. In *NAACL-HLT*, 2019. 3, 4, 12

[16] Alexey Dosovitskiy, Lucas Beyer, Alexander Kolesnikov, Dirk Weissenborn, Xiaohua Zhai, Thomas Unterthiner, Mostafa Dehghani, Matthias Minderer, Georg Heigold, Sylvain Gelly, et al. An image is worth 16x16 words: Trans-

formers for image recognition at scale. In *ICLR*, 2021. 3, 4
[17] Yinglin Duan, Tianyang Shi, Zhengxia Zou, Yenan Lin, Zhehui Qian, Bohan Zhang, and Yi Yuan. Single-shot motion completion with transformer. *arXiv:2103.00776*, 2021. 2
[18] Le Fang, Tao Zeng, Chaochun Liu, Liefeng Bo, Wen Dong, and Changyou Chen. Transformer-based conditional variational autoencoder for controllable story generation. *arXiv:2101.00828*, 2021. 3
[19] K. Fragkiadaki, S. Levine, Panna Felsen, and Jitendra Malik. Recurrent network models for human dynamics. In *ICCV*, 2015. 2
[20] R. P. Futrelle and G. C. Speckert. Extraction of motion data by interactive processin. In *IEEE Conf. Pattern Recog. and Image Processing*, 1978. 2
[21] Aphrodite Galata, N. Johnson, and David C. Hogg. Learning variable-length markov models of behavior. *CVIU*, 2001. 2
[22] D. Gavrila. The visual analysis of human movement: A survey. *CVIU*, 73:82–98, 1999. 2
[23] Ian Goodfellow, Jean Pouget-Abadie, Mehdi Mirza, Bing Xu, David Warde-Farley, Sherjil Ozair, Aaron Courville, and Yoshua Bengio. Generative adversarial nets. In *NeurIPS*, 2014. 2
[24] Chuan Guo, Xinxin Zuo, Sen Wang, Shihao Zou, Qingyao Sun, Annan Deng, Minglun Gong, and Li Cheng. Action2Motion: Conditioned generation of 3D human motions. In *ACMMM*, 2020. 2, 3, 5, 7, 12
[25] I. Habibie, Daniel Holden, Jonathan Schwarz, Joe Yearsley, and T. Komura. A recurrent variational autoencoder for human motion synthesis. In *BMVC*, 2017. 1, 2
[26] Félix G. Harvey, Mike Yurick, Derek Nowrouzezahrai, and Christopher Pal. Robust motion in-betweening. *ACM Trans. Graph.*, 39(4), 2020. 2
[27] Dan Hendrycks and Kevin Gimpel. Gaussian error linear units (GELUs). *arXiv:1606.08415*, 2016. 12
[28] Daniel Holden, Oussama Kanoun, Maksym Perepichka, and Tiberiu Popa. Learned motion matching. *ACM Trans. Graph.*, 2020. 3
[29] Daniel Holden, T. Komura, and J. Saito. Phase-functioned neural networks for character control. *ACM Transactions on Graphics (TOG)*, 36:1 – 13, 2017. 1, 3
[30] Catalin Ionescu, Dragos Papava, Vlad Olaru, and Cristian Sminchisescu. Human3.6M: Large scale datasets and predictive methods for 3D human sensing in natural environments. *IEEE Transactions on Pattern Analysis and Machine Intelligence*, 2014. 2
[31] Yanli Ji, Feixiang Xu, Yang Yang, Fumin Shen, Hen Tao Shen, and Weishi Zheng. A large-scale RGB-D database for arbitrary-view human action recognition. In *ACMMM*, 2018. 2, 5, 7
[32] J. Jiang, G. G. Xia, D. B. Carlton, C. N. Anderson, and R. H. Miyakawa. Transformer VAE: A hierarchical model for structure-aware and interpretable music representation learning. In *ICASSP*, 2020. 3
[33] Angjoo Kanazawa, Jason Y. Zhang, Panna Felsen, and Jitendra Malik. Learning 3D human dynamics from video. In *CVPR*, 2019. 3
[34] Diederik P Kingma and Max Welling. Auto-encoding variational bayes. In *ICLR*, 2014. 2, 4
[35] Muhammed Kocabas, Nikos Athanasiou, and Michael J. Black. VIBE: Video inference for human body pose and shape estimation. In *CVPR*, 2020. 2, 3, 8
[36] Hsin-Ying Lee, Xiaodong Yang, Ming-Yu Liu, Ting-Chun Wang, Yu-Ding Lu, Ming-Hsuan Yang, and Jan Kautz. Dancing to music. In *NeurIPS*, 2019. 2
[37] Jiaman Li, Yihang Yin, Hang Chu, Y. Zhou, Tingwu Wang, S. Fidler, and H. Li. Learning to generate diverse dance motions with transformer. *arXiv:2008.08171*, 2020. 2
[38] Ruilong Li, Shan Yang, David A. Ross, and Angjoo Kanazawa. Learn to dance with AIST++: Music conditioned 3D dance generation. *arXiv:2101.08779*, 2021. 2
[39] X. Lin and M. Amer. Human motion modeling using DVGANs. *arXiv:1804.10652*, 2018. 2
[40] Zhaojiang Lin, Genta Indra Winata, Peng Xu, Zihan Liu, and Pascale Fung. Variational transformers for diverse response generation. *arXiv:2003.12738*, 2020. 3
[41] Jun Liu, Amir Shahroudy, Mauricio Perez, Gang Wang, Ling-Yu Duan, and Alex C. Kot. NTU RGB+D 120: A large-scale benchmark for 3D human activity understanding. *IEEE Transactions on Pattern Analysis and Machine Intelligence*, 2019. 5
[42] Matthew Loper, Naureen Mahmood, Javier Romero, Gerard Pons-Moll, and Michael J. Black. SMPL: A skinned multi-person linear model. In *SIGGRAPH Asia*, 2015. 1, 3, 4
[43] Zhengyi Luo, S. Golestaneh, and Kris M. Kitani. 3D human motion estimation via motion compression and refinement. In *ACCV*, 2020. 3
[44] Naureen Mahmood, Nima Ghorbani, Nikolaus F. Troje, Gerard Pons-Moll, and Michael J. Black. AMASS: Archive of motion capture as surface shapes. In *ICCV*, 2019. 2
[45] Julieta Martinez, Michael J. Black, and Javier Romero. On human motion prediction using recurrent neural networks. In *CVPR*, 2017. 2
[46] Ben Mildenhall, Pratul P. Srinivasan, Matthew Tancik, Jonathan T. Barron, Ravi Ramamoorthi, and Ren Ng. NeRF: Representing scenes as neural radiance fields for view synthesis. In *ECCV*, 2020. 2
[47] D. Ormoneit, M. J. Black, T. Hastie, and H. Kjellström. Representing cyclic human motion using functional analysis. *Image and Vision Computing*, 23(14):1264–1276, 2005. 2
[48] J. O'Rourke and N. I. Badler. Model-based image analysis of human motion using constraint propagation. *IEEE Transactions on Pattern Analysis and Machine Intelligence*, 1980. 2
[49] Adam Paszke, Sam Gross, Francisco Massa, Adam Lerer, James Bradbury, Gregory Chanan, Trevor Killeen, Zeming Lin, Natalia Gimelshein, Luca Antiga, Alban Desmaison, Andreas Kopf, Edward Yang, Zachary DeVito, Martin Raison, Alykhan Tejani, Sasank Chilamkurthy, Benoit Steiner, Lu Fang, Junjie Bai, and Soumith Chintala. PyTorch: An imperative style, high-performance deep learning library. In *NeurIPS*, 2019. 12
[50] Georgios Pavlakos, Vasileios Choutas, Nima Ghorbani, Timo Bolkart, Ahmed A. A. Osman, Dimitrios Tzionas, and Michael J. Black. Expressive body capture: 3D hands, face, and body from a single image. In *CVPR*, 2019. 12
[51] Dario Pavllo, David Grangier, and M. Auli. QuaterNet: A quaternion-based recurrent model for human motion. In *BMVC*, 2018. 2
[52] Nikhila Ravi, Jeremy Reizenstein, David Novotny, Taylor Gordon, Wan-Yen Lo, Justin Johnson, and Georgia

Gkioxari. Accelerating 3D deep learning with PyTorch3D. *arXiv:2007.08501*, 2020. 12

[53] Amir Shahroudy, Jun Liu, Tian-Tsong Ng, and Gang Wang. NTU RGB+D: A large scale dataset for 3D human activity analysis. In *CVPR*, 2016. 5

[54] Kihyuk Sohn, Honglak Lee, and Xinchen Yan. Learning structured output representation using deep conditional generative models. In *NeurIPS*, 2015. 4

[55] S. Starke, H. Zhang, T. Komura, and J. Saito. Neural state machine for character-scene interactions. *ACM Transactions on Graphics (TOG)*, 38:1 – 14, 2019. 1, 3

[56] Sergey Tulyakov, Ming-Yu Liu, Xiaodong Yang, and Jan Kautz. MoCoGAN: Decomposing motion and content for video generation. In *CVPR*, 2018. 7

[57] Raquel Urtasun, David J. Fleet, and Neil D. Lawrence. Modeling human locomotion with topologically constrained latent variable models. In Ahmed Elgammal, Bodo Rosenhahn, and Reinhard Klette, editors, *Human Motion – Understanding, Modeling, Capture and Animation*, pages 104–118, Berlin, Heidelberg, 2007. Springer Berlin Heidelberg. 2

[58] Gül Varol, Ivan Laptev, Cordelia Schmid, and Andrew Zisserman. Synthetic humans for action recognition from unseen viewpoints. *arXiv:1912.04070*, 2019. 2, 6

[59] Sijie Yan, Zhizhong Li, Yuanjun Xiong, Huahan Yan, and Dahua Lin. Convolutional sequence generation for skeleton-based action synthesis. In *ICCV*, 2019. 2

[60] Sijie Yan, Yuanjun Xiong, and Dahua Lin. Spatial temporal graph convolutional networks for skeleton-based action recognition. In *AAAI*, 2018. 7

[61] Ye Yuan and Kris Kitani. Dlow: Diversifying latent flows for diverse human motion prediction. In *ECCV*, 2020. 1, 2

[62] Y. Zhang, Michael J. Black, and Siyu Tang. Perpetual motion: Generating unbounded human motion. *arXiv:2007.13886*, 2020. 2

[63] Y. Zhang, Michael J. Black, and Siyu Tang. We are more than our joints: Predicting how 3D bodies move. *arXiv:2012.00619*, 2020. 1, 2

[64] Rui Zhao, Hui Su, and Qiang Ji. Bayesian adversarial human motion synthesis. In *CVPR*, 2020. 3

[65] Y. Zhou, Connelly Barnes, Jingwan Lu, Jimei Yang, and H. Li. On the continuity of rotation representations in neural networks. In *CVPR*, 2019. 4, 5, 12, 13

[66] Shihao Zou, Xinxin Zuo, Yiming Qian, Sen Wang, Chi Xu, Minglun Gong, and Li Cheng. 3D human shape reconstruction from a polarization image. In *ECCV*, 2020. 5

APPENDIX

This document provides additional experiments (Section A), additional qualitative results (Section B), and implementation details (Section C).

A. Additional experiments

We ablate the model and vary key parameters to evaluate the influence of design choices on the quality of the results. In particular, we present results on the effect of λ_{KL} (Section A.1), batch size (Section A.2), number of layers (Section A.3), and the rotation representation for SMPL pose parameters (Section A.4).

A.1. Weight of the KL loss

As explained in Section 3.2 of the main paper, we empirically show the importance of the weighting between the reconstruction loss and the KL loss, controlled by λ_{KL}. Table A.1 presents results for several values of λ_{KL} and we find that there is a trade-off between diversity and realism that is best balanced at $\lambda_{KL} = 1\text{e}{-5}$. We use this value in all our experiments.

A.2. Influence of the batch size

As pointed out in Section 3.2 of the main paper, we find that the batch size significantly influences the performance. In Table A.2, we report results with batch sizes of 10, 20, 30, 40 for a fixed learning rate. The best performance is obtained at 20, which is used in all our experiments.

A.3. Number of layers

We experiment with the number of Transformer layers in both of our encoder and decoder architectures. Table A.3 summarizes the results. While 2 and 4 layers are suboptimal, the performance difference between 6 and 8 layers is minimal. We use 8 layers in all our experiments.

A.4. SMPL pose parameter representation

In Table A.4, we explore different rotation representations for SMPL pose parameters. Note that we also preserve the loss on the vertices $\mathcal{L}_V$ in all rows. We find that an axis-angle representation is difficult to train due to discontinuities, while others, such as quaternions, rotation matrices and 6D continuous representations [65] are similar in performance on NTU-13. On UESTC, we obtain the best performance with the 6D representation and use this in all our experiments.

B. Additional qualitative results

Figure A.1 demonstrates the diversity of our generated motions for additional actions on NTU-13 and UESTC.
Video. We provide a supplemental video at [1] to illustrate qualitatively the diversity in our generations and compare with Action2Motion [24]. Moreover, we visualize the effect of using a combined reconstruction loss defined both on rotations and vertex coordinates, as opposed to a single loss. We further present results of changing the duration of the generations. We also inspect the latent space by interpolating the noise vector. Finally, we present the denoising capability of our model by encoding-decoding through our latent space. This takes jerky motions and produces smooth but natural looking motion.

C. Implementation details

Architectural details. For all our experiments, we set the embedding dimensionality to 256. In the Transformer, we set the number of layers to 8, the number of heads in multihead attention to 4, the dropout rate to 0.1 and the dimension of the intermediate feedforward network to 1024. As in GPT-3 [10] and BERT [15], we use Gaussian Linear Error Units (GELU) [27] in our Transformer architecture.
Library credits. Our models are implemented with PyTorch [49], and we use PyTorch3D [52] to perform differentiable conversion between rotation representations. We integrate the differentiable SMPL layer using the PyTorch implementation of SMPL-X [50].
Metrics. For the evaluation metrics, we use the implementations provided by Action2Motion [24].
Runtime. Training takes 24 hours for 2K epochs on NTU, 19h hours for 5K epochs on HumanAct12, and 33 hours for 1K epochs on UESTC on a single Tesla V100 GPU, using 4GB GPU memory with batch size 20.
Training with sequences of variable durations. As explained in Section 4.2 of the main paper, we finetune our model with variable-durations after pretraining on fixed-durations. For this, we restore the model weights from the fixed-duration pretraining and finetune for 100 additional epochs, with the same training hyperparameters.

	UESTC					NTU-13			
	FID$_{tr}$↓	FID$_{test}$↓	Acc.↑	Div.→	Multimod.→	FID$_{tr}$↓	Acc.↑	Div.→	Multimod.→
Real	$2.93^{\pm0.26}$	$2.79^{\pm0.29}$	$98.8^{\pm0.1}$	$33.34^{\pm0.32}$	$14.16^{\pm0.06}$	$0.02^{\pm0.00}$	$99.8^{\pm0.0}$	$7.07^{\pm0.02}$	$2.27^{\pm0.01}$
λ_{KL} = 1e−3	$460.72^{\pm90.36}$	$490.12^{\pm36.10}$	$34.4^{\pm1.4}$	$20.69^{\pm0.60}$	$1.25^{\pm0.00}$	$13.79^{\pm0.03}$	$46.6^{\pm0.7}$	$5.79^{\pm0.04}$	$1.53^{\pm0.01}$
λ_{KL} = 1e−4	$367.95^{\pm94.07}$	$390.68^{\pm41.02}$	$38.1^{\pm0.9}$	$20.91^{\pm0.38}$	$9.19^{\pm0.08}$	$9.90^{\pm0.02}$	$50.3^{\pm1.0}$	$6.15^{\pm0.04}$	$2.86^{\pm0.02}$
λ_{KL} = 1e−5	$20.02^{\pm1.79}$	$23.64^{\pm3.59}$	$90.5^{\pm0.4}$	$32.77^{\pm0.48}$	$14.64^{\pm0.07}$	$0.17^{\pm0.00}$	$96.4^{\pm0.2}$	$7.08^{\pm0.03}$	$2.12^{\pm0.01}$
λ_{KL} = 1e−6	$34.13^{\pm5.52}$	$39.74^{\pm3.57}$	$77.4^{\pm0.8}$	$29.60^{\pm0.35}$	$18.08^{\pm0.08}$	$13.83^{\pm0.03}$	$46.6^{\pm0.7}$	$5.78^{\pm0.04}$	$1.54^{\pm0.01}$
λ_{KL} = 1e−7	$80.05^{\pm7.71}$	$83.68^{\pm12.55}$	$47.1^{\pm2.1}$	$25.06^{\pm0.15}$	$19.96^{\pm0.08}$	$7.04^{\pm0.03}$	$43.0^{\pm2.1}$	$6.17^{\pm0.03}$	$4.18^{\pm0.01}$

Table A.1: **Weighting the KL loss term:** To obtain a good trade-off between diversity and realism, it is important to find the balance between the reconstruction loss term and the KL loss term in training. We set the weight λ_{KL} to 1e−5 in our training.

	UESTC					NTU-13			
	FID$_{tr}$↓	FID$_{test}$↓	Acc.↑	Div.→	Multimod.→	FID$_{tr}$↓	Acc.↑	Div.→	Multimod.→
Real	$2.93^{\pm0.26}$	$2.79^{\pm0.29}$	$98.8^{\pm0.1}$	$33.34^{\pm0.32}$	$14.16^{\pm0.06}$	$0.02^{\pm0.00}$	$99.8^{\pm0.0}$	$7.07^{\pm0.02}$	$2.27^{\pm0.01}$
Batch size = 10	$283.28^{\pm94.40}$	$309.15^{\pm33.90}$	$39.7^{\pm1.5}$	$23.24^{\pm0.43}$	$15.73^{\pm0.11}$	$13.95^{\pm0.03}$	$46.2^{\pm0.6}$	$5.77^{\pm0.05}$	$1.56^{\pm0.01}$
Batch size = 20	$20.02^{\pm1.79}$	$23.64^{\pm3.59}$	$90.5^{\pm0.4}$	$32.77^{\pm0.48}$	$14.64^{\pm0.07}$	$0.17^{\pm0.00}$	$96.4^{\pm0.2}$	$7.08^{\pm0.03}$	$2.12^{\pm0.01}$
Batch size = 30	$23.37^{\pm2.95}$	$26.06^{\pm1.28}$	$89.7^{\pm0.5}$	$32.07^{\pm0.58}$	$14.59^{\pm0.05}$	$0.18^{\pm0.00}$	$96.2^{\pm0.2}$	$7.07^{\pm0.04}$	$2.13^{\pm0.01}$
Batch size = 40	$25.36^{\pm1.82}$	$28.22^{\pm2.16}$	$89.2^{\pm0.7}$	$32.22^{\pm0.44}$	$14.52^{\pm0.10}$	$0.26^{\pm0.00}$	$95.4^{\pm0.1}$	$7.06^{\pm0.05}$	$2.10^{\pm0.01}$

Table A.2: **Batch size:** We observe sensitivity of the Transformer VAE training to different batch sizes and report performances at several batch size values. We set this hyperparameter to 20 in our training.

	UESTC					NTU-13			
	FID$_{tr}$↓	FID$_{test}$↓	Acc.↑	Div.→	Multimod.→	FID$_{tr}$↓	Acc.↑	Div.→	Multimod.→
Real	$2.93^{\pm0.26}$	$2.79^{\pm0.29}$	$98.8^{\pm0.1}$	$33.34^{\pm0.32}$	$14.16^{\pm0.06}$	$0.02^{\pm0.00}$	$99.8^{\pm0.0}$	$7.07^{\pm0.02}$	$2.27^{\pm0.01}$
2-layers	$34.66^{\pm2.58}$	$37.17^{\pm3.53}$	$84.9^{\pm0.6}$	$30.87^{\pm0.36}$	$15.83^{\pm0.08}$	$0.24^{\pm0.00}$	$94.6^{\pm0.2}$	$7.07^{\pm0.03}$	$2.22^{\pm0.01}$
4-layers	$23.93^{\pm1.50}$	$26.75^{\pm1.99}$	$88.9^{\pm0.5}$	$32.24^{\pm0.76}$	$15.06^{\pm0.06}$	$0.19^{\pm0.00}$	$96.1^{\pm0.2}$	$7.09^{\pm0.04}$	$2.10^{\pm0.01}$
6-layers	$21.68^{\pm1.78}$	$24.92^{\pm2.09}$	$89.0^{\pm0.6}$	$32.61^{\pm0.41}$	$15.31^{\pm0.05}$	$0.16^{\pm0.00}$	$96.6^{\pm0.1}$	$7.09^{\pm0.04}$	$2.11^{\pm0.01}$
8-layers	$20.02^{\pm1.79}$	$23.64^{\pm3.59}$	$90.5^{\pm0.4}$	$32.77^{\pm0.48}$	$14.64^{\pm0.07}$	$0.17^{\pm0.00}$	$96.4^{\pm0.2}$	$7.08^{\pm0.03}$	$2.12^{\pm0.01}$

Table A.3: **Number of layers:** We use 8 layers in both the encoder and the decoder of the Transformer VAE. While the performance degrades at 2 or 4 layers, we see marginal gains after 6 layers.

	UESTC					NTU-13			
	FID$_{tr}$↓	FID$_{test}$↓	Acc.↑	Div.→	Multimod.→	FID$_{tr}$↓	Acc.↑	Div.→	Multimod.→
Real	$2.93^{\pm0.26}$	$2.79^{\pm0.29}$	$98.8^{\pm0.1}$	$33.34^{\pm0.32}$	$14.16^{\pm0.06}$	$0.02^{\pm0.00}$	$99.8^{\pm0.0}$	$7.07^{\pm0.02}$	$2.27^{\pm0.01}$
Axis-angle	$513.39^{\pm98.35}$	$531.88^{\pm43.41}$	$16.4^{\pm0.4}$	$19.75^{\pm0.44}$	$1.81^{\pm0.00}$	$14.98^{\pm0.03}$	$41.7^{\pm0.7}$	$5.29^{\pm0.02}$	$1.96^{\pm0.01}$
Quaternion	$281.9^{\pm87.5}$	$305.02^{\pm21.97}$	$41.2^{\pm1.0}$	$23.48^{\pm0.39}$	$14.57^{\pm0.06}$	$0.20^{\pm0.00}$	$95.6^{\pm0.3}$	$7.08^{\pm0.04}$	$2.23^{\pm0.01}$
Rotation matrix	$277.14^{\pm76.59}$	$300.29^{\pm29.53}$	$41.6^{\pm1.9}$	$22.25^{\pm0.30}$	$14.56^{\pm0.10}$	$0.17^{\pm0.00}$	$95.9^{\pm0.2}$	$7.08^{\pm0.04}$	$2.19^{\pm0.01}$
6D continuous	$20.02^{\pm1.79}$	$23.64^{\pm3.59}$	$90.5^{\pm0.4}$	$32.77^{\pm0.48}$	$14.64^{\pm0.07}$	$0.17^{\pm0.00}$	$96.4^{\pm0.2}$	$7.08^{\pm0.03}$	$2.12^{\pm0.01}$

Table A.4: **SMPL pose parameter representation:** We investigate different rotation representations for the SMPL pose parameters. While on NTU-13, all except axis-angle representations perform similarly, the best performing representation on UESTC is the 6D continuous representation [65]. Note that the action recognition model which is used for evaluation is based on 6D rotations on UESTC and joint coordinates on NTU-13. Therefore, we convert each generation to these representations before evaluation.

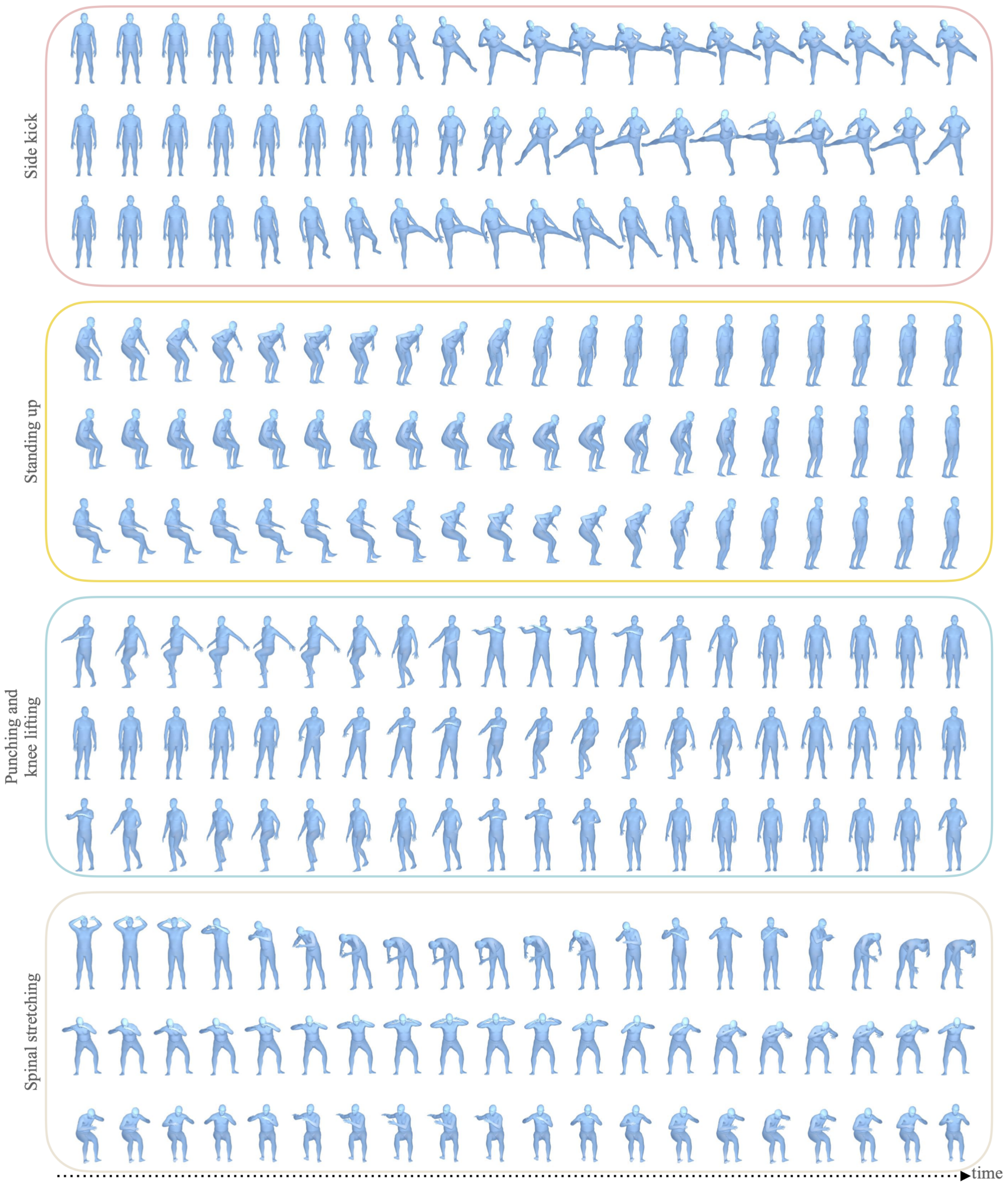

Figure A.1: **Additional qualitative results:** We provide more action categories from NTU-13 (top two actions: 'Side kick' and 'Standing up') and UESTC (bottom two actions: 'Punching and knee lifting' and 'Spinal stretching'). As in Section 5 of the main paper, we show 3 generations per action. Our model generates different ways to perform the same action.